

An optical leaky wave antenna with Si perturbations inside a resonator for enhanced optical control of the radiation

Salvatore Campione, Caner Guclu, Qi Song, Ozdal Boyraz, and Filippo Capolino *

Department of Electrical Engineering and Computer Science, University of California, Irvine, California 92697, USA

*f.capolino@uci.edu

<http://capolino.eng.uci.edu>

Abstract: We investigate the directive radiation at 1550 nm from an optical leaky wave antenna (OLWA) with semiconductor perturbations made of silicon (Si). We study the radiation pattern dependence on the physical dimensions, number of perturbations and carrier densities in these semiconductor perturbations through optical excitations at a visible wavelength, 625 nm. In this detailed theoretical study we show the correlation between the pump power absorbed in the perturbations, the signal guided in the waveguide and the radiation through leakage. To overcome the limited control of the radiation intensity through excess carrier generation in Si, we present a new design with the OLWA integrated with a Fabry-Pérot resonator (FPR). We provide analytical and numerical studies of the enhanced radiation performance of the OLWA antenna inside the FPR, and derive closed-form formulas accounting for LW reflection at the edges of the FPR. A discussion on the constructive and destructive radiation by the direct and reflected leaky waves in the FPR resonator is provided. Results shown in this paper exhibit 3 dB variation of the radiation and pave the way for further optimization and theoretical developments.

©2012 Optical Society of America

OCIS codes: (230.7390) Waveguides, planar; (050.6624) Subwavelength structures; (050.2230) Fabry-Pérot.

References and links

1. P. Ghenuche, S. Cherukulappurath, T. H. Taminiau, N. F. van Hulst, and R. Quidant, "Spectroscopic mode mapping of resonant plasmon nanoantennas," *Phys. Rev. Lett.* **101**(11), 116805 (2008).
2. R. L. Olmon, P. M. Krenz, A. C. Jones, G. D. Boreman, and M. B. Raschke, "Near-field imaging of optical antenna modes in the mid-infrared," *Opt. Express* **16**(25), 20295–20305 (2008).
3. Q. Song, F. Qian, E. K. Tien, I. Tomov, J. Meyer, X. Z. Sang, and O. Boyraz, "Imaging by silicon on insulator waveguides," *Appl. Phys. Lett.* **94**(23), 231101 (2009).
4. Q. Song, S. Campione, O. Boyraz, and F. Capolino, "Silicon-based optical leaky wave antenna with narrow beam radiation," *Opt. Express* **19**(9), 8735–8749 (2011).
5. A. A. Oliner, "Leaky-wave antennas," in *Antenna Engineering Handbook*, R. C. Johnson, ed. (McGraw Hill, 1993).
6. D. R. Jackson and A. A. Oliner, "Leaky-wave antennas," in *Modern Antenna Handbook*, C. A. Balanis, ed. (Wiley, 2008), 325–367.
7. D. R. Jackson, J. Chen, R. Qiang, F. Capolino, and A. A. Oliner, "The role of leaky plasmon waves in the directive beaming of light through a subwavelength aperture," *Opt. Express* **16**(26), 21271–21281 (2008).
8. K. Van Acoleyen, W. Bogaerts, J. Jägeršká, N. Le Thomas, R. Houdré, and R. Baets, "Off-chip beam steering with a one-dimensional optical phased array on silicon-on-insulator," *Opt. Lett.* **34**(9), 1477–1479 (2009).
9. E. K. Tien, X. Z. Sang, F. Qing, Q. Song, and O. Boyraz, "Ultrafast pulse characterization using cross phase modulation in silicon," *Appl. Phys. Lett.* **95**(5), 051101 (2009).
10. A. Gondarenko, J. S. Levy, and M. Lipson, "High confinement micron-scale silicon nitride high Q ring resonator," *Opt. Express* **17**(14), 11366–11370 (2009).
11. S. M. Sze and K. K. Ng, *Physics of Semiconductor Devices* (Wiley, 2006).

12. O. Boyraz, X. Sang, E. Tien, Q. Song, F. Qian, and M. Akdas, "Silicon based optical pulse shaping and characterization," Proc. SPIE **7212**, 72120U, 72120U–13 (2009).
13. D. Dimitropoulos, R. Jhaveri, R. Claps, J. C. S. Woo, and B. Jalali, "Lifetime of photogenerated carriers in silicon-on-insulator rib waveguides," Appl. Phys. Lett. **86**(7), 071115 (2005).
14. Y. Dan, K. Seo, K. Takei, J. H. Meza, A. Javey, and K. B. Crozier, "Dramatic reduction of surface recombination by in situ surface passivation of silicon nanowires," Nano Lett. **11**(6), 2527–2532 (2011).
15. T. Dittrich, T. Bitzer, T. Rada, V. Y. Timoshenko, and J. Rappich, "Non-radiative recombination at reconstructed Si surfaces," Solid-State Electron. **46**(11), 1863–1872 (2002).
16. F. M. Schuurmans, A. Schonecker, J. A. Eikelboom, and W. C. Sinke, "Crystal-orientation dependence of surface recombination velocity for silicon nitride passivated silicon wafers," in *Photovoltaic Specialists Conference, 1996., Conference Record of the Twenty Fifth IEEE* (1996), 485–488.
17. S. Paulotto, P. Baccarelli, F. Frezza, and D. R. Jackson, "A novel technique for open-stopband suppression in 1-D periodic printed leaky-wave antennas," IEEE Trans. Antenn. Propag. **57**(7), 1894–1906 (2009).

1. Introduction

Optical antennas have the potential to boost the efficiency of optoelectronic devices [1,2]. For some applications, e.g., planar imaging [3], there is the need of very directive near-IR optical antennas with controlled radiation power density and beam steering. We have recently introduced in [4] a CMOS compatible optical leaky wave antenna (OLWA) that provides directive radiation at 1550 nm, through the excitation of a leaky wave (LW) guided mode [5–7] in a dielectric waveguide comprising periodic perturbations made of semiconductors, such as silicon. The tunability of the optical parameters of silicon (such as refractive index and absorption coefficient) via electronic or optical excess carrier generation renders itself a possible platform for optical antennas that can facilitate radiation intensity control [8]. Especially, the optical carrier generation technique enables an all-optical-integrated device which alleviates the system complexity and cost by removing the circuitry of the electronic injection.

The goal of this paper is to investigate how and to what extent we can control the LW radiation by changing the optical properties of semiconductor perturbations through optical excitations. In particular, this work provides an investigation of the radiation dependence on the number and on the physical dimensions of the perturbations at the signal wavelength λ_s and on the carrier generation due to optical absorption at a pump wavelength λ_p . We start analyzing the directive radiation of the OLWA at the signal wavelength $\lambda_s = 1550$ nm, in absence of any pump. Then, we study the distribution of optical pump intensity at $\lambda_p = 625$ nm in silicon perturbations for the cases of unidirectional pump co-propagating with the signal (Fig. 1) and bidirectional pump cases. We also estimate the amount of pump power absorbed in the perturbations, guided in the waveguide and radiated through leakage. Initial estimates show a weak tunability of the radiation intensity, at a fixed direction, at λ_s , mainly because of the very limited area where Si is present. However, one should notice that having very small Si perturbations has the advantage to allow very fast electronic/optical control of the carrier generation, because carriers do not penetrate into the dielectric waveguide.

In order to overcome the problem of limited tunability, we analyze the case of an OLWA embedded into a Fabry-Pérot resonator (FPR) and show that the control of the radiation intensity at a fixed direction can be greatly enhanced. The theoretical aspects of a LW radiator inside a resonator are here studied for the first time, and closed-form formulas are provided to explain this new concept. A proper combination of the FPR length and the OLWA length leads to few dBs of tunability of the radiation intensity, paving the way to new possible ways of enhanced control of LW radiation. In this work we focus on the two dimensional (2D) model (invariant along z) of the antenna reported in Fig. 1, because the agreement between 2D and 3D calculations has been previously shown in [4].

The structure of the paper is as follows. The OLWA structure is reported in Sec. 2, together with a study on how the size and number of perturbations affect its radiation

properties. Then, in Sec. 3, we introduce the optical control of the radiation, which provides with the excess carrier generation and limited radiation control discussed in Secs. 4 and 5, respectively. Therefore, in Sec. 6, we embed the OLWA into a FPR to achieve enhanced control of the radiation intensity and we derive closed-form formulas that parameterize the radiation in terms of the LW propagation and attenuation constants. Conclusions are reported in Sec. 7.

2. Optical leaky wave antenna: proposed structure and perturbation study

The OLWA is basically made of a perturbed waveguide, i.e., comprising silicon (Si) perturbations (Fig. 1). The waveguide is made of silicon nitride (Si_3N_4) with refractive index $n_w = 1.67$, is positioned along the x direction and is $100\ \mu\text{m}$ long; it has a width $w = 1\ \mu\text{m}$. The Si_3N_4 waveguide is sandwiched between two silica glass (SiO_2) domains with equal width of $9.5\ \mu\text{m}$, with refractive index $n_h = 1.45$. The structure has then a total width of $20\ \mu\text{m}$ in the y direction. The remaining space is assumed to be free space with unity refractive index. To provide directive radiation, we utilize N silicon (Si) perturbations, with refractive index n_{Si} (which is a frequency dependent parameter), positioned periodically along the x direction on the bottom side of the Si_3N_4 waveguide, and symmetrically with respect to the center of the waveguide (along x). The unit cell of the perturbed waveguide is represented with a dashed red box in Fig. 1. We want to specify that in architecture point of view we are dealing with a periodic structure made of small silicon perturbations in a silicon nitride waveguide that radiates according to LW theory [4], as described above. In conventional approaches one has either pure semiconductor waveguides [9] or pure dielectric waveguides [10]. Here, the proposed work deals with a dielectric waveguide with semiconductor perturbations. Hence, one can control the carriers in the perturbation regions only and, importantly, carriers do not penetrate into the waveguide. Due to this feature and the low semiconductor volume, the introduced device has the potential of high speed operation.

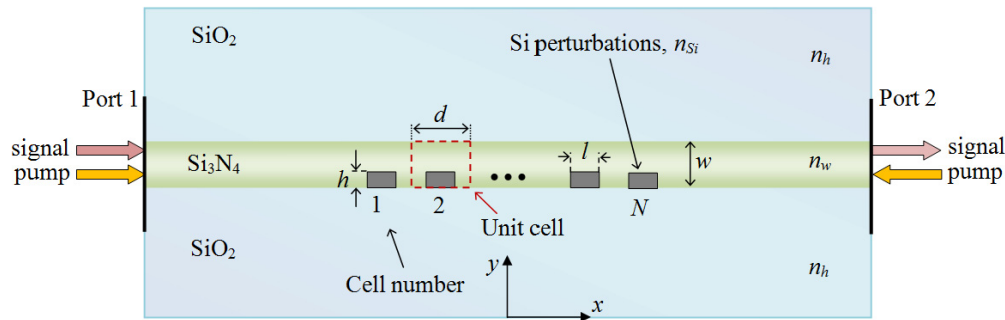


Fig. 1. 2D model of the proposed OLWA, including dimensions, and the optical pumping scheme.

We analyze two possible sets of Si perturbations. The first set, referred to as Set 1 (same unit cell as in [4], but with different overall antenna dimensions), has $l = 485\ \text{nm}$, $h = 300\ \text{nm}$, and $d = 970\ \text{nm}$ (refer to Fig. 1). The second set, with stronger perturbations, referred to as Set 2, has $l = 500\ \text{nm}$, $h = 500\ \text{nm}$ and $d = 1030\ \text{nm}$. Both designs aim at achieving high directivity at the bottom “broadside” direction, i.e., along the $-\hat{y}$. All the simulations in Figs. 2-3 and 5-7 are carried out using full-wave simulation software employing the finite element method in frequency domain (High frequency structure simulator, HFSS by Ansys Inc., and COMSOL Multiphysics by COMSOL Group) which provide good agreement of the results.

A guided wave (signal) is injected from the left side (simulated port size is $2.4\ \mu\text{m}$) of the antenna at the free space wavelength $\lambda_s = 1550\ \text{nm}$, with electric field polarized along z .

When this guided wave encounters the waveguide region comprising the periodic silicon perturbations, it transitions into a LW, slowly decaying while traveling along the perturbed waveguide. The purpose of the periodic perturbations is to create a radiating $n = -1$ Floquet spatial harmonic [4] with wavenumber $k_{x,-1} = \beta_{-1} + i\alpha$, with $\beta_{-1} = \beta_0 - 2\pi/d$ where β_0 is the fundamental wavenumber in the perturbed waveguide. When using small perturbations the value of β_0 is close to that of the mode wavenumber β in the unperturbed (i.e., without Si perturbations) waveguide. We want to specify that in theoretical point of view we develop the radiation theory of OLWAs based on leaky wave approach [4]. The two leaky wave parameters β_{-1} and α are strongly used here to explain the radiation phenomenon, also in the case when the OLWA is embedded into a FPR, as described in Sec. 6.

The LW radiation will determine the directive radiation pattern as in Fig. 2(a) in free space, previously confirmed against two theoretical methods in [4] using Set 1 with $N = 60$ (with $n_{Si} = 3.48$ and negligible losses), which results in $\beta_{-1}/k_s \approx -0.059$ and $\alpha/k_s \approx 0.011$, where $k_s = 2\pi/\lambda_s$ is the signal free space wavenumber. Some power is radiated in a very directive beam with half-power beamwidth (HPBW) of about 1.4° , with maximum radiation at $\phi_M \approx -93.4^\circ$. The radiation in the $+\hat{y}$ direction ($\phi_M \approx 93.4^\circ$) is about 4 dB lower than the one in $-\hat{y}$ direction ($\phi_M \approx -93.4^\circ$). Radiation in the region $0^\circ < \phi < 180^\circ$ can be avoided by adding reflectors. When using Set 2, the maximum radiation is at $\phi_M \approx -92.5^\circ$, and the LW parameters are $\beta_{-1}/k_s \approx -0.046$ and $\alpha/k_s \approx 0.011$. The radiation in the $+\hat{y}$ direction ($\phi_M \approx 92.5^\circ$) is about 17 dB lower than the one in $-\hat{y}$ direction ($\phi_M \approx -92.5^\circ$). Note however that comparable side lobe levels are observed when using the two sets (refer to Fig. 2(a)). We compute also the directivity of the two antennas, defined as

$$D = \frac{\max[U(\phi)]}{\frac{1}{2\pi} \int_0^{2\pi} U(\phi) d\phi} \quad (1)$$

where $U(\phi) = |E_{FF}(\rho, \phi)|^2 \rho / (2\eta_0)$, $E_{FF}(\rho, \phi)$ is the far-zone electric field, evaluated for very large $\rho = \sqrt{x^2 + y^2}$, the observer distance from the origin of the coordinate system on the x - y plane, and $\eta_0 = \sqrt{\mu_0 / \epsilon_0} \approx 377\Omega$ is the free space impedance.

The plot of the radiation pattern $U(\phi)$ for Set 1, normalized to its maximum value, is reported in Fig. 2(a) at the signal wavelength λ_s , retrieved via full-wave simulation (COMSOL Multiphysics), leading to a directivity $D = 17.5$ dB. Corresponding data for Set 2 lead to a directivity $D = 15.1$ dB. (Alternatively, one could calculate D by using the Stratton-Chu formulation as was done in [4], leading to a slightly lower value, because the contribution of the lateral edges in Fig. 1 was neglected.) These results are a clear indication that the device here proposed is an efficient optical antenna, able to produce very directive beams (Fig. 2(a), as well as the discussion in Fig. 3). Note that we are using the 2D model in Fig. 1, thus we are integrating only with respect to the angle ϕ and the normalization scheme uses an isotropic radiator on the x - y plane only.

We show in Fig. 3 how the number of perturbations N (set to 30, 40, 50, and 60), as well as the dimensions of the Si perturbations (Set 1 and Set 2, see insets in Fig. 3) affects the performance of the OLWA. Scattering parameters S_{11} and S_{12} are very small for both Set 1 and Set 2.

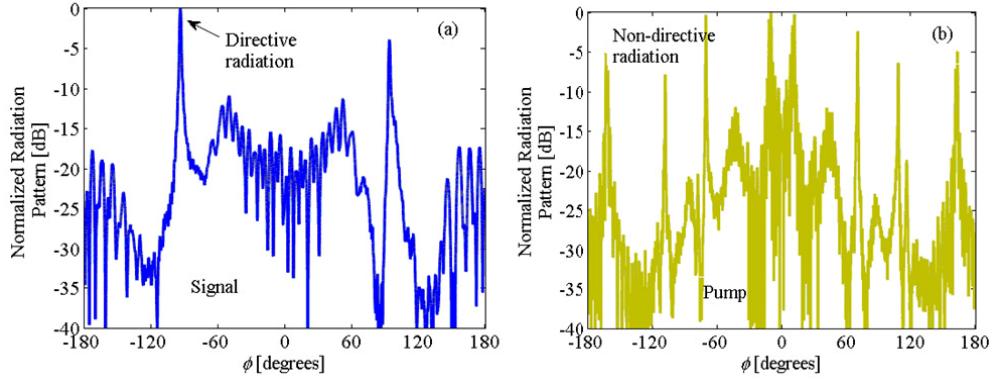


Fig. 2. Normalized radiation pattern at (a) signal and (b) pump wavelengths, for Set 1. Result retrieved with COMSOL. A similar plot is attainable for Set 2 (not shown). Maximum signal radiation is at $\phi_M = -93.4^\circ$.

Reflection S_{11} is nearly unaffected by the number of perturbations ranging from 30 to 60. Instead, both the transmission coefficient S_{12} and the HPBW decrease for increasing N (showing indeed that a long perturbation section is desired to achieve very directive radiation, with an HPBW of about 1.4° for Set 1 with $N = 60$). Set 1 provides with a slightly more directive radiation (i.e., smaller HPBW) than Set 2. Note that small values of S_{11} and S_{12} (both less than -15 dB, in both cases) for any N imply that the signal power radiated by the perturbed waveguide region will be close in value to the incident power furnished by the incoming signal wave mode at the input.

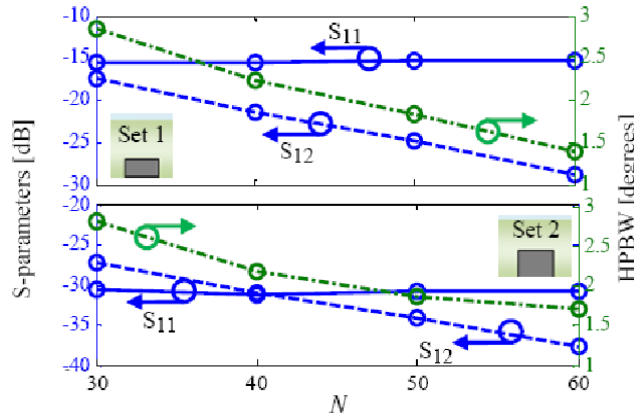


Fig. 3. Scattering parameters and half power beamwidth (HPBW) versus number of perturbations N for Set 1 and Set 2. Results retrieved with COMSOL (in agreement with HFSS, not shown for clarity).

3. Modeling of optical pumping schemes

As previously mentioned, the LW radiation at λ_s can be controlled by changing the optical properties of silicon perturbations. One of the approaches that can be used to tune the optical properties of silicon is the use of optical pumping at wavelength λ_p where silicon is absorbing. To this aim, we select the pump excitation to be at the optical wavelength $\lambda_p = 625$ nm where Si has high absorption ($n_{Si} \approx 3.89 + i1.65 \times 10^{-2}$ [11]) and low cost lasers are readily available. As shown in Fig. 1, we utilize two pumps, one co-propagating and one

counter-propagating with respect to the signal. These two pumps are used to generate electron-hole pairs in the silicon perturbations, almost uniformly along the OLWA, that can alter both the real (Δn_{Si}) and the imaginary (Δk_{Si}) parts of the Si complex refractive index (unitless) at λ_s as described by the Drude's model [12]. Accordingly,

$$\begin{aligned}\Delta n_{Si}(N_e, N_h) &= -(8.8 \times 10^{-4} N_e + 8.5 N_h^{0.8}) \times 10^{-18}, \\ \Delta k_{Si}(N_e, N_h) &= (8.5 N_e + 6.0 N_h) \times 10^{-16} / k_s,\end{aligned}\quad (2)$$

where N_e and N_h are the concentrations of electrons and holes (in cm^{-3}) in Si, generated through photon absorption ($N_e = N_h$ since one photon generates an electron-hole pair), with k_s in m^{-1} . The concentrations of electrons and holes in each Si perturbation are computed through the absorbed power in each perturbation ($P_{\text{abs,Si}}$) at the visible pumping light of 625 nm as

$$N_e = N_h = \frac{P_{\text{abs,Si}}}{\hbar\omega} \times \frac{\tau}{V}, \quad (3)$$

where $\hbar\omega$ is the photon energy in Joule at 625 nm, τ is the average lifetime of the electrons and holes in seconds and V is the volume of the silicon perturbation.

Here the average carrier lifetime τ is determined by the surface recombination effects as described in [13]. Because of the abrupt termination of the Si crystal, there are a large number of electrically active states at the interfaces Si/SiO₂ and Si/Si₃N₄. These unpassivated interfaces typically contain a large number of carrier recombination centers which cause a fast surface recombination effect that significantly shortens the lifetime of carriers accumulated in submicron size semiconductor devices [14]. We assume that the antenna is invariant along z , thus no diffusion takes place in that direction. The calculation of the carrier lifetime τ requires the solution of the 2D steady state continuity equation on the x - y cross section of a Si perturbation, where the average lifetime τ is mainly due to the surface recombination effect.

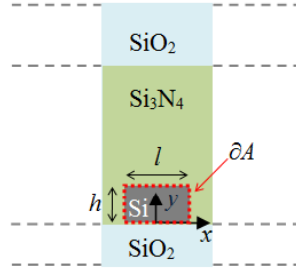


Fig. 4. Unit cell of the waveguide in Fig. 1, showing the Si perturbation.

In the analytical model in [13], the 2D steady state continuity equation is

$$\oint_{\partial A} S n dl = \int_A \left(G - \frac{n}{\tau_b} \right) dA \quad (4)$$

where S is the interface recombination velocity (length per time), dl is the differential length along the contour ∂A (the red dotted contour in Fig. 4) that encloses A , the area of the x - y cross-section of the Si perturbation excited by the pump light. Moreover, G is the photon-induced volume generation rate (per volume per time), used in the lifetime calculation,

$\tau_b = 1$ ms is the bulk silicon recombination lifetime, and n is the electron or hole carrier concentration (per volume). For the Si perturbation area A within the red dotted contour shown in Fig. 4, the photon-induced generation rate G and the carrier concentration n are assumed to be uniformly distributed. The continuity Eq. (4) is then rewritten as

$$S_{\text{Si-SiO}_2}nl + S_{\text{Si-Si}_3\text{N}_4}n(2h+l) = \left(G - \frac{n}{\tau_b}\right)lh, \quad (5)$$

where the generation rate can be expressed in terms of the average carrier lifetime as $G = n/\tau$. Therefore, the average carrier lifetime is calculated as

$$\frac{1}{\tau} = \frac{1}{\tau_b} + \frac{S_{\text{Si-SiO}_2}}{h} + \frac{S_{\text{Si-Si}_3\text{N}_4}(2h+l)}{lh}. \quad (6)$$

When using Set 1 geometry, $l = 0.485$ μm , $h = 0.3$ μm , $S_{\text{Si-SiO}_2} = 8000$ cm/s, and $S_{\text{Si-Si}_3\text{N}_4} = 1000$ cm/s [15,16], the carriers in Si perturbation have an average lifetime $\tau = 2.93$ ns.

4. Carrier generation due to the power absorbed by the Si perturbations at the pump wavelength

Accordingly, considering a structure with $N = 60$ perturbations, assume now to inject a pump input power density of about 0.14 MW/cm² at the free space wavelength $\lambda_p = 625$ nm, and assume to adopt either a single pump or a bidirectional pump scheme (Fig. 1). The injected pump power will be split in three parts: (i) some part will be guided in the waveguide; (ii) some part will be absorbed by the silicon perturbations (and will generate excess carriers); and (iii) some part will be radiated away in free space, as shown in Fig. 2(b), in a non-directive fashion (we recall the pump is not used for direct radiation purposes, but only to generate excess carriers in Si that will be used to control the radiation at the signal wavelength of 1550 nm). These pump power fractions versus cell number (Fig. 1) adopting Set 1 are shown in Fig. 5(a) for single pump, and in Fig. 5(b) for bidirectional pump configuration (normalized with respect to the furnished pump power P_{pump}). Notice that implicitly, in the case of a single pump, there is a power conversion efficiency dictated by the geometry as $\eta = P_{\text{abs,Si}}/P_g$, where P_g is the pump power delivered to a cell (Fig. 1) and $P_{\text{abs,Si}}$ is the pump power absorbed by the Si perturbation in that cell. Due to the radiation and absorption, weaker field will reach successive Si perturbations, which will then absorb less power than previous ones, explaining the decaying trend in Fig. 5(a). Similarly, in the bidirectional case, not all the injected pump power is used to generate excess carriers. However, this case is used to approximately make every Si perturbation absorb the same amount of power. Under the same assumptions of Fig. 5, the profile of excess carrier concentration in Si perturbations versus cell number is shown in Fig. 6(a) for single pump, and in Fig. 6(b) for bidirectional pump configuration, after having applied Eq. (3). Note the agreement between the two full-wave results.

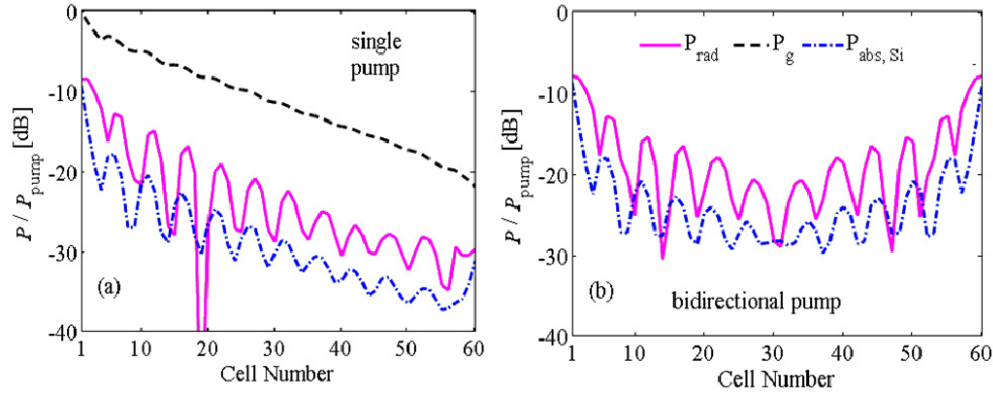


Fig. 5. Guided (delivered to a cell), radiated and absorbed (inside the Si perturbation) power at 625 nm versus cell number, in case of (a) single and (b) bidirectional pump schemes for Set 1. A similar plot is attainable for Set 2 (not shown). Result retrieved with full-wave simulator HFSS (in agreement with COMSOL, not shown for clarity).

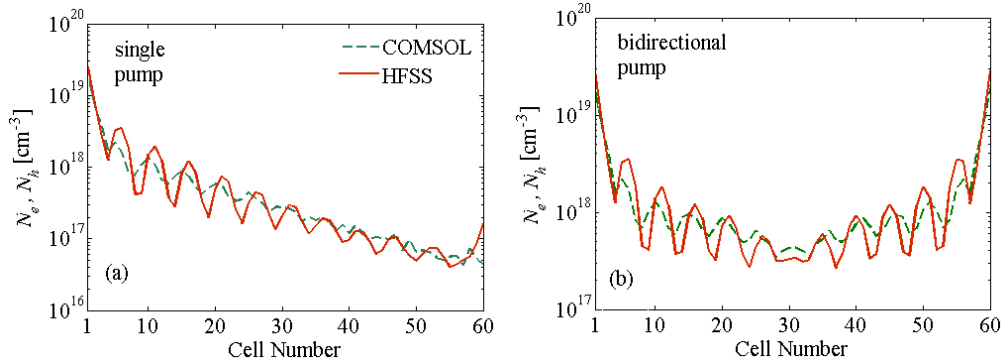


Fig. 6. Excess carrier concentration versus cell number for (a) single and (b) bidirectional pump schemes for Set 1, obtained by both COMSOL and HFSS simulations. A similar plot is attainable for Set 2 (not shown).

5. Strength of radiation pattern control

Looking at the result in Fig. 6(b), one can assume that the carrier concentration generated by the bidirectional pump scheme is almost constant in every silicon perturbation (thanks to the symmetry of the structure). Then the pump power level could be adjusted to achieve a desired excess electron-hole concentration. As an example, one can use Eq. (2) with $N_e = N_h = 5 \times 10^{18} \text{ cm}^{-3}$ and $N_e = N_h = 10^{19} \text{ cm}^{-3}$, and compute the Si complex refractive index at 1550 nm in the two cases, which are equal to $n_{\text{Si}} \approx 3.468 + i1.79 \times 10^{-3}$ and $n_{\text{Si}} \approx 3.458 + i3.58 \times 10^{-3}$, respectively. The far field radiation pattern can then be computed in absence and presence of optical pumping, and the result with respect to the generated excess carrier concentration is shown in Fig. 7 by both COMSOL and HFSS full-wave simulations, in very good agreement. Note that the directivity variation is negligible when excess carriers are present, as can be inferred from the plot in Fig. 7. Moreover, we observe that radiation maximum intensity (e.g., around -93.4° with no pump, red curve), slightly decreases for increasing excess carrier concentration (caused by increasing pump), as shown with the dashed green and dashed-dotted blue curves. This variation is limited to a fraction of a dB and it is due to the increase of $\text{Im}(n_{\text{Si}})$ in the very small Si perturbations. Furthermore, we also notice that the beam slightly moves towards more negative angles for increasing

pumping power due to the variation of β_{-1} . This result is in agreement with the small perturbation model reported in [4].

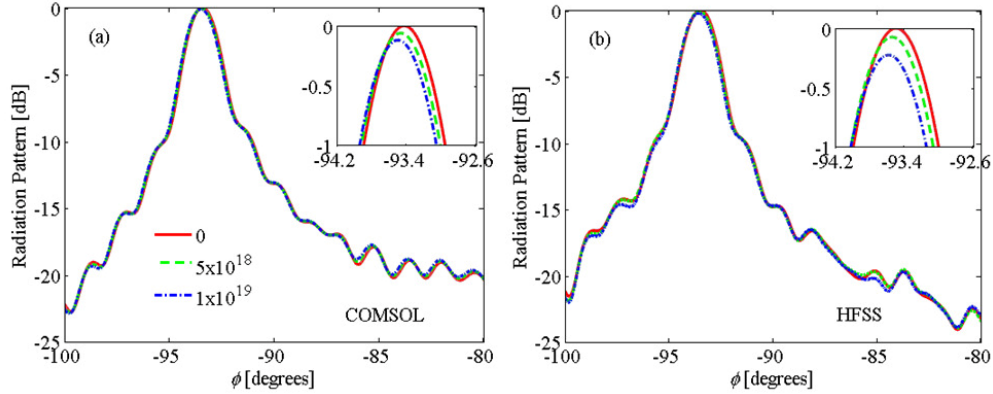


Fig. 7. Radiation pattern in absence and in presence of optical pumping that provides the excess carrier concentrations $N_e = N_h$ given in the legend (in cm^{-3}). Agreement between (a) COMSOL and (b) HFSS full-wave simulations. The insets show the limited variation in radiation (fraction of a dB) caused by the excess carriers.

These results show that optical control of an isolated OLWA is possible but rather limited. Therefore effective tunable scenarios are foreseen with control enhanced by integrating the OLWA inside a Fabry-Pérot resonator in the next section.

6. Enhanced control via integration of the OLWA into a Fabry-Pérot resonator

In this section, we provide the theoretical model useful for the estimation of the radiation of an OLWA integrated into a Fabry-Pérot resonator as shown in Fig. 8. The selectivity of the FPR renders the OLWA radiation more sensitive to the presence of excess carriers in the Si perturbations, as explained in the following. To the authors' knowledge, the theory of a leaky wave radiator inside a resonator has not been developed yet, and here we provide closed-form formulas to explain this concept for the first time.

Assume a LW inside the resonator excited at the signal frequency through the partially reflective mirror 1 in Fig. 8, and reflected back at mirror 2. A LW in a perturbed waveguide can be in general represented as a sum of spatial harmonics, as shown in Eq. (1) in [4]; however, at a certain distance y from the waveguide, the LW field is dominated by its radiating $n = -1$ Floquet spatial harmonic. The radiating LW field in the periodic section of the OLWA inside the resonator, polarized along z , is represented as the summation of two LWs' spatial $n = -1$ harmonics (taking into account all multiple reflections), E^+ traveling along $+x$ and E^- traveling along $-x$, whose expressions for x between $-Nd/2$ and $Nd/2$ are

$$E^+(x) = f_{\text{FPR}} E(x), \quad E^-(x) = f_{\text{FPR}} \Gamma_0 E(-x), \quad (7)$$

with

$$E(x) = E_0 e^{-\alpha x} e^{i\beta_{-1}x}, \quad \Gamma_0 = \Gamma_2 e^{-\alpha Nd} e^{i\beta_{-1}Nd} e^{i\beta_2 D_2}. \quad (8)$$

The term E_0 represents the amplitude of the field, polarized along z , of the resulting wave traveling towards the $+x$ direction inside the resonator, defined at $x = 0$ (assumed to be the center of the perturbed waveguide, for simplicity) at a certain distance y from the waveguide, and

$$f_{\text{FPR}} = \frac{1}{1 - \Gamma_1 \Gamma_2 e^{-2\alpha Nd} e^{2i\beta_{-1}Nd} e^{2i\beta(D_1+D_2)}}. \quad (9)$$

The terms Γ_1 and Γ_2 are the complex reflection coefficients at mirrors 1 and 2, respectively, D_1 and D_2 are the lengths of the two unperturbed waveguides, shown in Fig. 8. The coefficient Γ_0 is the reflection coefficient towards the $+x$ direction, referred to the center $x = 0$, and its magnitude depends on the LW attenuation constant α ; the term f_{FPR} accounts for the infinite summation of multiple reflections due to the resonator and plays an important role in the LW control enhancement. All the other parameters in Eqs. (7)-(9) have been previously defined in Sec. 2. Each LW radiation depends on the LW parameters α and β_{-1} , as well as on the resonator factor f_{FPR} which assumes a large value at the Fabry-Pérot resonance and affects the overall field strength.

The total OLWA far-zone electric field at a general location (ρ, ϕ) , where ρ is the observer distance from the origin of the coordinate system on the x - y plane, is obtained by superposition of the two LW radiations as

$$E_{\text{FF}}^{\text{T}}(\rho, \phi) = f_{\text{FPR}} \left[E_{\text{FF}}^+(\rho, \phi) + \Gamma_0 E_{\text{FF}}^-(\rho, \phi) \right]. \quad (10)$$

Here, each LW far-field radiation E_{FF}^{\pm} is obtained by integrating the LW field $E(\pm x)$ in Eq. (7) over the antenna ‘‘aperture’’, defined as the contour from where we assume radiation is propagating away, e.g., here defined by the dashed red contour in Fig. 8 at the interface between silica glass and free space, as shown in [4,6,7].

Accordingly, each LW radiated field has the closed-form expression $E_{\text{FF}}^{\pm}(\rho, \phi) = F^{\pm}(\phi) e^{ik_s \rho} / \sqrt{\rho}$, where field radiation patterns are defined as

$$F^{\pm}(\phi) = E_0 e^{-i\pi/4} \sqrt{\frac{k_s}{2\pi}} Nd \sin \phi \frac{\sin \psi^{\pm}}{\psi^{\pm}} \quad (11)$$

with

$$\psi^{\pm} = (k_s \cos \phi \mp \beta_{-1} \mp i\alpha) Nd / 2, \quad (12)$$

and k_s is the wavenumber at the signal frequency in the surrounding free space. The total OLWA field radiation pattern is obtained by superposition of the two LW field radiation patterns as

$$F^{\text{T}}(\phi) = f_{\text{FPR}} \left[F^+(\phi) + \Gamma_0 F^-(\phi) \right], \quad (13)$$

which is related to the power radiation pattern in Sec. 2 by $U(\phi) = |F^{\text{T}}(\phi)|^2 / (2\eta_0)$.

One can infer from Eq. (13) that Γ_0 can be set such that the beams F^{\pm} interfere in a constructive manner at a desired direction.

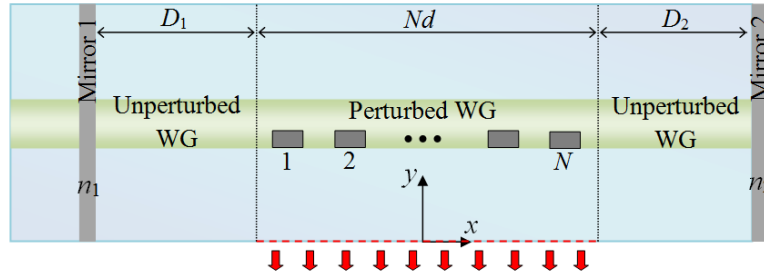


Fig. 8. OLWA embedded into a Fabry-Pérot resonator limited by two partially reflective mirrors. The distances D_1 and D_2 need to be carefully determined using LW theory, in such a way that the two LWs traveling in opposite directions in the OLWA section produce beams with constructive interference.

The directivity of each LW radiation F^\pm increases with increasing number of perturbations, as previously shown in Fig. 3 (higher N implies longer perturbed waveguide). However, the larger N is, the more attenuated the forward leaky wave E^+ is, diminishing the global effect of the resonator. Indeed, the LW attenuation constant α affects the quality factor of the FPR. Therefore, it is apparent that there is a trade-off between the LW directivity, proportional to the number N of Si perturbations, and the enhancement f_{FPR} achieved through the FPR. In other words, the length of the OLWA inside the FPR has to be smaller than an isolated OLWA (i.e., there are fewer perturbations) and this is necessary to design the FPR with low losses and a high quality factor. To illustrate the overall performance of the OLWA in the FPR, we design the FPR in Fig. 8 to be at resonance at the chosen operating signal wavelength of $\lambda_s = 1550$ nm, assuming absence of excess carriers. We then suppose to have excess carriers ($N_e = N_h = 10^{19}$ cm $^{-3}$) generated in the Si perturbation either by optical pumping as discussed in Sec. 3, or by current injection. Because of the FPR, the presence of excess carriers highly affects the value of f_{FPR} , and thus the structure falls quickly out of resonance, enhancing the limited control observed in Fig. 7. Indeed, the utilization of FPR manifests itself through input mismatch; i.e., through carrier injection, the FPR is pushed out of resonance and thus the radiated signal level is modified significantly. In presence of excess carriers, β_{-1} and α , to be used in Eqs. (11)-(12), are computed as in Sec. 5 in [4] using the small perturbation model. The relative variations of the leaky wave propagation constant β_{-1} and of the attenuation constant α , due to the presence of excess carriers in Si, are reported in Table 1 normalized with respect to the value of $|k_{x,-1}|$ in absence of carrier injection.

We analyze the three cases outlined in Table 1: Set 1 and Set 2 (as in Sec. 2), and Potential case (the periodicity of the perturbations is $d = 970$ nm). We use the following common parameters: $\Gamma_1 = 0.984 \angle -162^\circ$, $\Gamma_2 = 0.997 \angle -164^\circ$ (assuming to have silver mirrors with a thickness of 30 nm and 100 nm, respectively), the unperturbed waveguide made of the same materials as in Fig. 1 and $N = 15$. The radiation patterns F^Γ for the three cases with and without excess carriers are shown in Fig. 9. These are computed using Eq. (13) and normalized with respect to the maximum of the curve in absence of excess carriers, for each case. These maxima occur at the following angles: $\phi_{\text{Set 1}} = -92.1^\circ$, $\phi_{\text{Set 2}} = -91.2^\circ$, $\phi_{\text{Pot. Case}} = -90.3^\circ$. For these three cases, the directivity and HPBW before the introduction of excess carriers are reported in Table 1. When introducing excess carriers, both the directivity and HPBW are not found to be much different from the values in Table 1 for each case. This

result shows that neither the introduction of the FPR nor the Si absorption affect much the directivity of the antenna.

Table 1. Parameters of the OLWA Designs Integrated into FPR

Parameter	Set 1	Set 2	Potential Case
α / k_S	0.0105	0.0111	0.005
β_{-1} / k_S	-0.0594	-0.0457	-0.02
$\Delta\alpha / k_{x,-1} $	0.89%	1.85%	2.6%
$\Delta\beta_{-1} / k_{x,-1} $	-5.54%	-11.49%	-16.2%
D_1	913 nm	870 nm	770 nm
D_2	1461 nm	1411 nm	1278 nm
Si filling factor	0.15	0.24	0.15
D	13.7 dB	14.6 dB	14.7 dB
HPBW	7°	6.2°	5.5°

We want to highlight that when we introduce excess carriers we are interested in the level modulation of the radiated signal at a fixed direction. This variation due to either absence or presence of excess carriers is about 1.3 dB, 2 dB and 3 dB for the three cases in Table 1, respectively. This result clearly shows the advantages of embedding an OLWA into a Fabry-Pérot resonator because the control is significantly enhanced with respect to the result in the previous section. We want to remark that the goal of this paper is not to control beam steering; rather we look at modifying and controlling radiation at a fixed direction, which varies a few dBs. This paves the way for further improvement and future devices based on this principle, as for example very fast optical switches, etc.

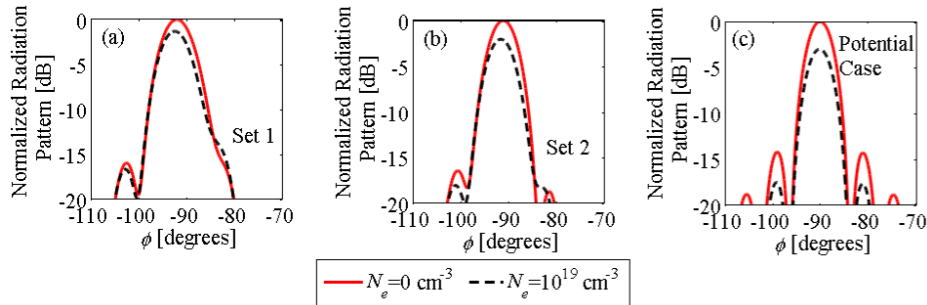


Fig. 9. Radiation pattern of an OLWA embedded into an FPR with (dashed black) and without (solid red) excess carrier injection in the Si perturbations using three different designs: (a) Set 1, (b) Set 2, and (c) Potential Case.

7. Conclusion

We analyze the radiation principle and performance of an optical leaky wave antenna (OLWA), analyzing the radiation dependence on the number of perturbations and their physical dimensions. Then, we analyze optical pumping schemes by propagating visible light at 625 nm (in the Si bandgap) together with the signal to generate electron and hole excess carriers in the small Si perturbations. This results in a limited control of the leaky wave radiation intensity at 1550 nm. To overcome the limited control we embed the OLWA inside a Fabry-Pérot resonator and observe enhancements in the order of 3 dB variation. We foresee values as high as 10 dB with proper realistic designs. Therefore this paper shows that this is a promising strategy for enhanced electrical or optical control of the OLWA radiation. This result is not negligible and thus it offers novel promising control capabilities that might allow the generation of very fast optical switches, as an example. It is important to note that the Si

perturbation dimensions have to be minimal for two main reasons; (1) enabling very fast control because electron hole carriers are limited to a very small region and do not penetrate the dielectric waveguide, and (2) enabling very small leaky wave attenuation constant α , key point to exploit the resonator properties as well as describing radiation intensity, beamwidth, radiation angle, etc. via closed-form formulas. Theoretical developments and further understanding of the radiation by LW antennas inside resonators is required to better exploit or optimize the control possibility. Also, effective tunable scenarios are foreseen also by exploiting strong input mismatch caused by the open-stopband [17] of modes in the periodically perturbed waveguide.

Acknowledgments

This work is supported by the National Science Foundation Award # ECCS-1028727. The authors also thank Ansys Inc. for providing HFSS, and COMSOL Group for COMSOL Multiphysics.